Applied Magnetic Resonance
https://doi.org/10.1007/s00723-024-01716-1

Applied
Magnetic Resonance

RESEARCH

Electron-Spin Relaxation of S_3^- in Ultramarine Blue and Lapis Lazuli

Sandra S. Eaton[1] · Debbie G. Mitchell[1] · Gareth R. Eaton[1]

Received: 26 August 2024 / Revised: 26 August 2024 / Accepted: 7 September 2024

Abstract

The blue color that has made lazurite (lapis lazuli) a prized mineral is due to the same S_3^- radical that is in synthetic ultramarine blue (UMB), which has been proposed as a CW EPR standard. Continuous wave and pulsed EPR spectra and relaxation times of S_3^- are compared for three commercial sources of synthetic UMB, for samples of lapis lazuli from Afghanistan, Chile, Colorado USA, and Pakistan, and a solution in DMSO:dioxane. The spin concentrations in the UMB samples were high, in the range of 3×10^{20} to 5×10^{20} spins/g. The field-swept echo-detected spectra of UMB samples have lineshapes at 4.2 K that depend on the field at which phase adjustment is performed, indicating strong spin–spin interaction. The spectra of the minerals included large spectral contributions from Mn^{2+}, in addition to S_3^- for which the concentrations were 6×10^{18} to 2.9×10^{19} spins/g. Features in the spin-echo-detected spectra attributed to forbidden Mn^{2+} transitions were confirmed by comparison with Mn^{2+} spectra in CaO powder. Large distributions in relaxation times caused derived results to depend strongly on the experimental acquisition windows for echo decay and inversion-recovery curves. Short-phase memory times are attributed to spin–spin interactions and to motion of the S_3^- in the lattices. Relatively weak temperature dependence of spin lattice relaxation rates below or around 25 K is attributed to substantial spin–spin interaction and cross relaxation. The strong spin–spin interaction is not present for 0.4 mM S_3^- in DMSO:dioxane. The shorter T_1 for S_3^- than for SO_2^- or SO_3^- is attributed to stronger spin–orbit coupling.

✉ Gareth R. Eaton
geaton@du.edu

[1] Department of Chemistry and Biochemistry, University of Denver, Denver, CO 80210, USA

Published online: 10 September 2024

1 Introduction

The blue color of the mineral lapus lazuli and of ultramarine blue (UMB) is due to the radical S_3^-. The history of lapis lazuli (LL) and synthetic ultramarine pigments was surveyed by Seel [1]. The utility of S_3^- and S_2^- trapped in various zeolites as long-lasting pigments stimulates extensive studies of physical properties of synthetic ultramarines of various colors (see Fig. 22 in Ref. [2]). The EPR signal in UMB was identified as S_3^- by Gardner and Fraenkel [3]. Because of the stability of S_3^- in UMB, the strong continuous wave (CW) EPR signal at room temperature, and the separation of the g value of S_3^- (~2.028, Table S1) from the free-electron value, UMB has been suggested as a CW EPR standard [4]. Consequently, it is valuable to document the EPR spectra and relaxation times for well-defined samples, compare with prior results on UMB and LL samples, and extend interpretations of relaxation mechanisms. Our prior EPR study of UMB focused on the frequency dependence of CW linewidths [5]. Spin relaxation of S_3^- has been studied in synthetic UMB and its analogs [6–10]. Although there has been extensive study of synthetic UMB, the natural LL that are emulated by synthetic UMB have not been studied by pulsed EPR. In this study we report EPR spectra and electron-spin relaxation for three samples of synthetic UMB, four samples of natural LL, and a solution of S_3^- in DMSO:dioxane.

2 Experimental

UMB from Pfaltz & Bauer (product U00031) is designated as UMB-PB. A sample of UMB purchased by Dr. Ralph Weber, Bruker Biospin, from Spectrum Chemical Manufacturing Corporation is designated as UMB-Spec. Both suppliers reported that they have no record of the chemical composition. A third sample, found in a storage room at University of Denver, had been repackaged in a glass jar with a style and label that an on-line search indicates was produced about 100 years ago. We refer to this sample as UMB-old. The UMB samples were used as received.

The natural products we acquired were all provided as LL. The sample identified as from Afghanistan was sold by a local Denver store and is designated as LL-Afghan. The sample from a deposit in Colorado, USA, was purchased from Zacchariah Zypp (https://zypp.net/) in Crested Butte, Colorado and designated as LL-Colo. A sample from a deposit in Chile was provided by Prof. Filipe Herrera, Department of Physics, Universidad de Santiago de Chile and designated as LL-Chile. A sample from a deposit in Pakistan was provided by Prof. Velavan Kathirvelu, National Institute of Technology, Goa and designated as LL-Pakis. Although lazurite is a soft mineral, in LL it occurs with other minerals that make the rock hard. The rock samples were broken into fragments small enough to fit in quartz EPR tubes by hitting with a hammer and crushing with hand pliers. Fragments were selected that were intensely blue, but still have substantial admixtures of light-colored minerals mixed with the blue stone.

For comparison with the Mn^{2+} lines in the mineral samples, measurements were also made on the Mn^{2+} impurity in reagent grade CaO powder (Sigma-Aldrich 248568 lot 17201BJV).

A solution of S_3^- was prepared by the method of Li et al. [11]. A 1:1 mixture of 1,4-dioxane and DMSO (2 mL each, Sigma Aldrich) was prepared in a graduated cylinder and bubbled with nitrogen gas, using Teflon tubing. Potassium polysulfide (2.5 mg, K_2S_x Sigma Aldrich) was ground into smaller pieces with a mortar and pestle and added to the degassed solvent mixture. Nitrogen bubbling through the mixture was continued for ~ 15 min until the polysulfide had completely dissolved and the solution turned blue.

The presence of the S_3^- was confirmed through both UV–Vis and CW-EPR spectroscopy. The blue color and the $\lambda_{max} = 617$ nm indicate the presence of the $S_3^{\bullet-}$ radical [11]. The slight greenish cast to the blue and a band in the visible spectrum with $\lambda_{max} = 415$ nm indicate the presence of S_4^{2-} [11]. While collecting the CW-EPR on the EMX-nano, the sample (in ~ 1 mm ID Teflon tubing supported within a 4-mm quartz tube) was continually degassed with nitrogen. CW EPR confirmed the sulfur radical ($g = 2.025$) and using an internal standard, the concentration of sulfur radical was ~ 0.4 mM.

Each of the solid samples was placed in a standard ca. 3.9 mm o.d. (2.9 mm i.d.) fused quartz tube purchased from Wilmad Glass. The tubes were evacuated, back-filled with He gas at ca. 200 mTorr, and flame-sealed. The solution in DMSO:dioxane was deoxygenated by freeze–pump–thaw prior to back-filling with He gas and flame sealing. CW spectra at 295 K were acquired on a Bruker EMXnano with operating frequency about 9.65 GHz, 100 kHz modulation frequency and microwave power in the linear response regime. The spin concentrations for weighted aliquots of solids were measured using the spin-count software of the Bruker EMXnano spectrometer. CW spectra at cryogenic temperatures were acquired with a Bruker E580, 100 kHz modulation frequency, and microwave power in the linear response regime.

Pulsed EPR spectra and relaxation time data were acquired using a Bruker E580 spectrometer with an ER4118X-DM5 dielectric resonator at X-band. The spin echoes of the UMB and LL samples are intense, fully consistent with the measured spins per gram. A few 1 to 2 mm fragments in a standard EPR tube yielded echoes that did not require detection amplifier gain or signal averaging. T_m was measured with 2-pulse echo decays using a $\pi/2 - \tau - \pi - \tau -$ echo pulse sequence and 2-step phase cycling. T_1 was measured by 3-pulse inversion recovery with a $\pi - T_{pulse} - \pi/2 - \tau - \pi - \tau -$ echo pulse sequence in which T_{pulse} was stepped to monitor signal recovery. ESEEM data were collected at two magnetic field positions in the spectrum via a three-pulse sequence ($\pi/2 - \tau - \pi/2 - T - \pi/2 - \tau -$ echo). In this resonator the maximum echo for $S = ½$ is observed at 15 to 17 dB. The $S = 5/2$ Mn^{2+} signal required 9 dB less power.

The length of the $\pi/2$ pulse was 40 ns for most experiments, although $\pi/2$ pulse lengths up to 160 ns were used to check for instantaneous diffusion in the echo decays, and pulse lengths of 16 ns were used to decrease the impact of spectral diffusion on T_1 and to perform 3-pulse ESEEM. At 78 K the temperature was controlled by cold N_2 flow in a Bruker/Oxford CF935 cryostat.

Temperatures between 4.2 and 60 K were achieved using the same cryostat and a Bruker/ColdEdge Stinger closed cycle He refrigeration system. Temperature at the sample was measured with a Cernox sensor. By monitoring changes in echo amplitude it was evident that temperature equilibration was almost immediate.

Although distributions were observed for T_m, the short time constants and impact of instrumental deadtime caused us to use a single exponential fit, Eq. (1). Because of the substantial distributions in T_1, the inversion-recovery curves were fit with stretched exponentials Eq. (2).

$$Y(\tau) = Y(0)\exp\left(\frac{-2\tau}{T_m}\right) \tag{1}$$

$$Y(T) = Y(0)\left(-1 + \exp\left(\frac{-T}{T_1}\right)^{\beta}\right) \tag{2}$$

where $Y(0)$ is signal intensity at time = 0 and β is the stretch factor. The time constants calculated using either biexponential or stretched exponential fits depended strongly on the time window of the recorded data. Deletion of one or a few early time data points dramatically altered the derived values, which is symptomatic of contributions from components with short time constants that may be due to spectral diffusion. Approximations using two exponentials to fit the inversion-recovery data usually yielded two time constants differing by about an order of magnitude.

The temperature dependence of $1/T_1$ was modeled using Eq. (3), [12]

$$\frac{1}{T_1} = AT + A_{\mathrm{Ram}}\left(\frac{T}{\theta_D}\right)^9 J_8\left(\frac{\theta_D}{T}\right) + A_{\mathrm{loc}}\left[\frac{e^{\Delta_{\mathrm{loc}}/T}}{\left(e^{\Delta_{\mathrm{loc}}/T} - 1\right)^2}\right] \tag{3}$$

where A is an experimentally-determined adjustable parameter, T is temperature, A_{Ram} is an experimentally-determined adjustable parameter that scales the contribution from the 2-photon Raman process [13, 14], θ_{D} is the Debye temperature, J_8 is the transport integral Eq. (4), that was developed to model heat capacity, A_{loc} is an experimentally determined adjustable parameter that scales the contribution from the local mode, and Δ_{loc} is the energy of the local mode [15].

$$J_8\left(\frac{\theta_{\mathrm{D}}}{T}\right) = \int_0^{\theta_{\mathrm{D}}/T} x^8 \frac{e^x}{(e^x - 1)^2} dx \tag{4}$$

An approximately linear dependence of $1/T_1$ on temperature can occur in high-concentration samples, and is attributed to cross relaxation. In some publications this linear dependence is incorrectly labeled a direct process, from which it cannot be distinguished based solely on temperature dependence. The coefficient A in Eq. (3) includes the effects of both cross relaxation and the direct process.

3 Results and Discussion

3.1 CW and Echo-Detected Spectra of S_3^- in UMB

Room temperature X-band CW EPR spectra of the three synthetic UMB samples (Figs. 1 and S1) and for S_3^- in DMSO can be approximated with Lorentzian line widths, as previously reported for UMB-PB [5]. However, the lineshape is more complicated than a single Lorentzian. The simulations shown in Figs. 1 and S1 were obtained with anisotropic g values and anisotropic peak-to-peak line width ranging from about 10 to 100 G (Table S1). Since the g anisotropy is not resolved at room temperature, the three components of the g tensor are not defined, but

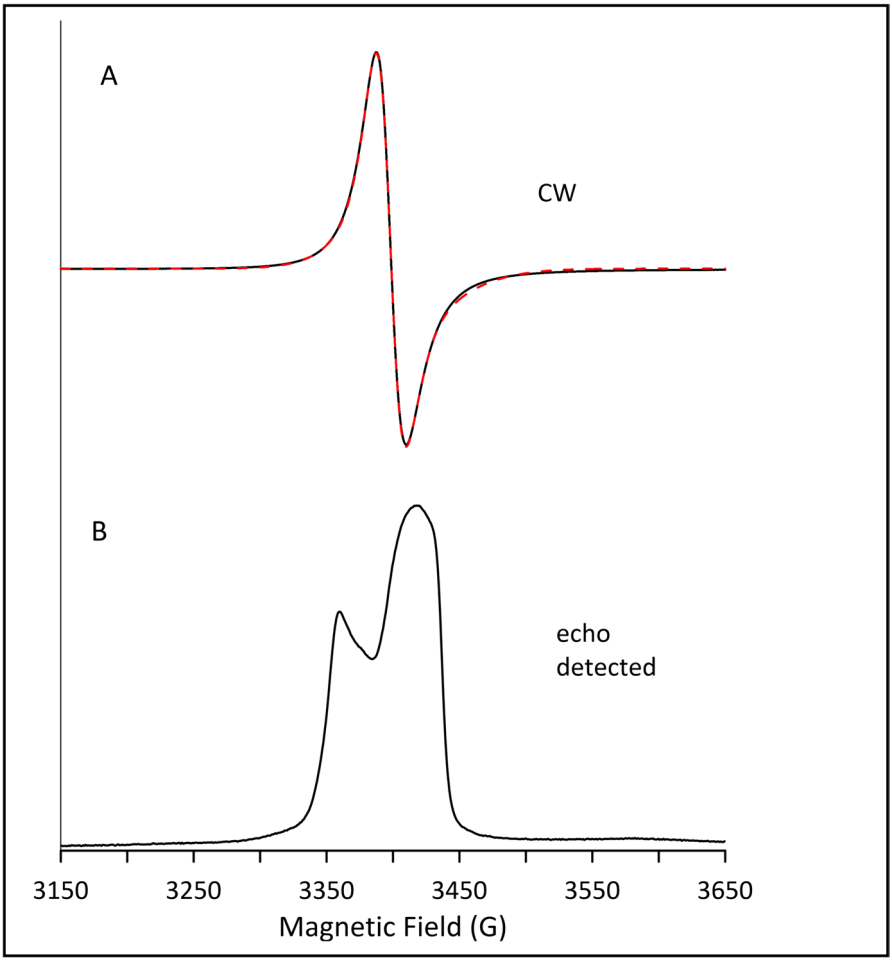

Fig. 1 Spectra of UMB-PB. **A** CW spectrum at 295 K (black line), with simulation (red dashed line). **B** Field-swept echo-detected spectrum at 9.8 K

averages are in the range reported for S_3^- in many sodalite and zeolite samples. The spin concentrations in the three UMB samples (Table 1) are between 3.2×10^{20} and 5.1×10^{20} spin/g. Wieckowski [16] reported that in the range 10^{18} to 10^{19} spins/g the CW EPR line width increased with concentration, and then between 10^{19} and 10^{20} spins/g the line width decreased due to exchange interactions. Gobeltz-Hautecoeur et al. [17] used copper sulfate and ruby crystal standards to estimate the S_3^- concentration in three UMB pigments. They found 1.0, 4.4, and $5.4\pm0.2\times10^{20}$ spins/g, corresponding to 0.08 to 0.43 spins per sodalite cage. Wieckowski [16] reported a 10 G linewidth for a synthetic UMB sample with 2×10^{20} spins/g and 5.9×10^{20} zeolite cells per gram, which corresponds to 0.34 ± 0.05 spins per cell. Comparison of the 5.1×10^{20} spins/g in our deeply blue UMB-PB sample with these literature reports indicates that the S_3^- in our sample occupy about half of the cages [17]. Our two other UMB samples have slightly lower spin concentration, but S_3^- radicals still occupy about a third of the cages, which is high enough to cause exchange narrowed lines at 295 K. Raulin et al. [18] reported 5×10^{19} S_2^- spins/g for an industrial green ultramarine, and 1 and 3×10^{19} spins/g for other pigments prepared from zeolites. Hoffmann et al. [10] reported 4×10^{16} spins/g in zeolite L, 3.3×10^{18} spins/g in zeolite A, and 3×10^{16} spins/g in cancrinite. The variations in spin concentration reflect the strong dependence on sample preparation.

CW and field-swept echo-detected spectra of the UMB samples were recorded at cryogenic temperatures. The echo-detected spectrum of UMB-PB at 9.8 K exhibits g anisotropy that is not detectable at 295 K (Fig. 1B). Temperature dependence of spectra of UMB have previously been reported between 77 and 376 K [6]. The loss of resolution in the room temperature spectra reveals dynamic averaging and exchange in the solid. A UMB based on zeolite A with 3.2×10^{17} spins per gram described in ref. [6] exhibited partial resolution of g anisotropy at 295 K, so in that case there was not full dynamic averaging or spin exchange at 295 K. Hoffman [8] observed broadening of the S_3^- spectra when warmed above 70 K. Hoffman et al. reported five spectral components with varying *g* values that were attributed to difference is local environments [9]. Field-swept echo-detected spectra of UMB-Spec at 9.4 K revealed underlying broad signals (Fig. S2A) that were not present in UMB-PB (Fig. 1B) or UMB-old (Fig. S2B).

Table 1 Spin concentrations in UMB and lapis lazuli samples

Sample	Spins per gram
UMB-Spec	3.23×10^{20}
UMB-old	3.76×10^{20}
UMB-PB	5.05×10^{20}
LL-Chile	6.29×10^{18}
LL-Afghan	1.46×10^{19}
LL-Pakis	2.90×10^{19}
LL-Colo	Undefined[a]

[a]The S_3^- signal in LL-Colo, was weak relative to the Mn^{2+} signals (Fig. S3A), so the spin concentration was not defined

The field-swept, echo-detected spectra in the UMB samples are about 100 G wide, which includes the wings of the derivative CW spectra. The amount of sample that could be used for spin echo measurements overwhelmed the spectrometer detection system when used for CW measurements, especially at low temperatures. It appears that different subsets of the distributions of spins are observed in pulse and CW measurements, with fewer spins detected after the instrumental dead-time of the pulse spectrometer.

A striking observation is that the shape of the anisotropic central 100 G of the echo-detected spectrum of S_3^- in UMB at 4.2 K depends strongly on the position in the spectrum at which the pulse phase is adjusted (Fig. 2). The phenomenon occurs at low temperature where the T_1 values are very long. Similar phase dependence was

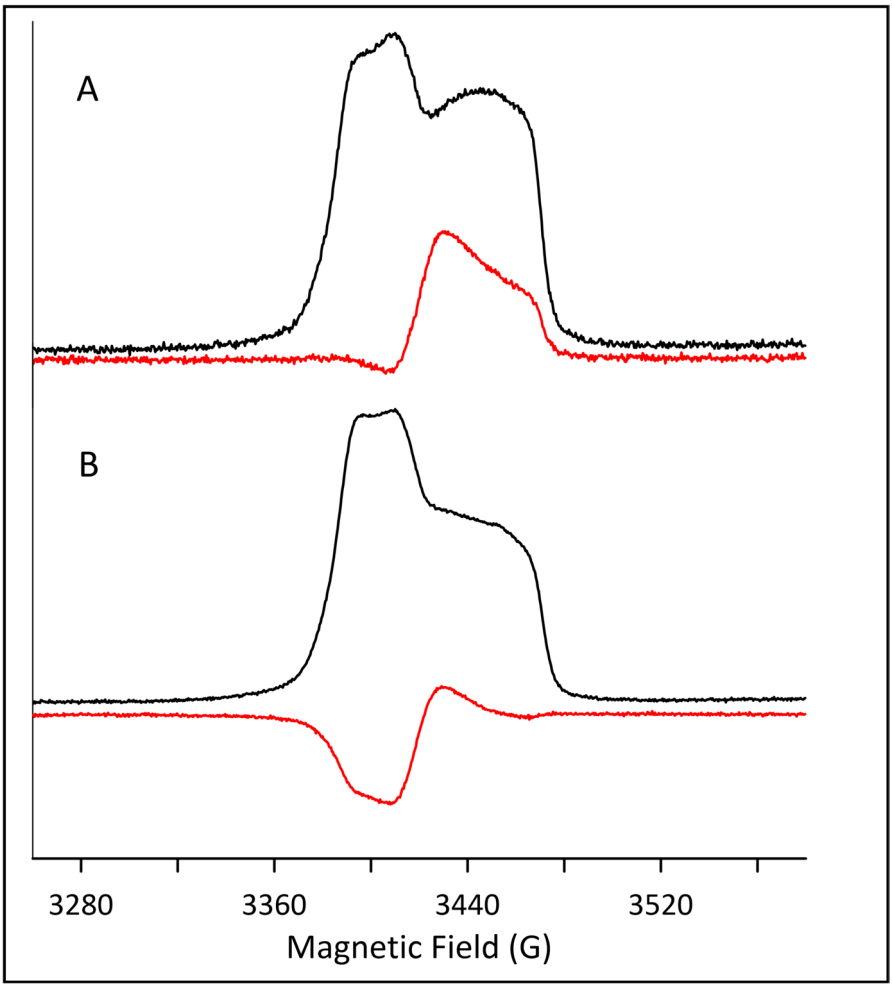

Fig. 2 UMB-PB **A** Phase adjusted at 3395G, in-phase channel (black), quadrature phase channel (red). **B** Phase adjusted at 3460 G in-phase channel (black), quadrature phase channel (red)

observed for the two other synthetic UMB samples, but not for the mineral samples. We attribute this sample dependence to lower S_3^- concentration in the mineral samples (Table 1). Consequently, the appearance of the spectra at about 4 K, including relative intensities, depend on pulse-repetition time relative to T_1 and on phasing. We speculate that this phase effect is analogous to the absorption/emission spectra observed in photoexcited triplets [19, 20]. Some subset of the S_3^- radicals are close to another S_3^- radical and at low temperatures have very long relaxation times—possibly many seconds. Excitation of one radical in a pair polarizes the other in the pair. One could anticipate similar observations for other radicals included in porous solids such as metal–organic-frameworks.

3.2 CW and Echo-Detected Spectra of Lapis Lazuli

Strong Mn^{2+} lines are superimposed on the S_3^- signals in CW spectra of the mineral samples. For LL-Pakis (Fig. 3) and LL-Afghan the S_3^- signal at 298 K is strong relative to the Mn^{2+} signal. However, for LL-Chile (Fig. 4) the overlap with the Mn^{2+} signals makes it difficult to quantitate the S_3^- and for LL-Colo (Fig. S3) the S_3^- signal 293 K is so weak relative to the Mn^{2+} lines that quantitation was not attempted. The concentration of S_3^- in the LL samples (Table S1) is one to two orders of magnitude smaller than for UMB. The lower average values are due in part to presence of other minerals in the samples, but may also reflect differences in the conditions under which the minerals were formed.

At 80 K the Mn^{2+} signals in the LL samples saturate more readily than the S_3^- signals so the S_3^- signal can be more readily distinguished in the CW spectrum of LL-Colo at 80 K than at 293 K (Fig. S3). Field-swept echo-detected spectra of LL-Afghan are shown in Fig. 5. When B_1 is optimized for $S=5/2$ the Mn^{2+} lines are emphasized (Fig. 5A), but when B_1 is optimized for S = ½ the S_3^- signal and the Mn^{2+} forbidden transitions are emphasized (Fig. 5B). Similar data for LL-Colo are shown in Fig. S4. The field-swept echo-detected spectrum of Mn^{2+} in CaO powder recorded at 81 K (Fig. S5) with B_1 optimized for $S=5/2$ is in good agreement with the experimental spectrum of Mn^{2+} doped into zinc formate [21]. When B_1 is optimized for $S=1/2$ the allowed Mn^{2+} transitions are nearly nulled and the forbidden transitions dominate the spectrum (Fig. S5B). The similarity between spectra in Fig. S5 and S6 confirms the assignment of the Mn^{2+} lines in the LL samples. Field-swept echo-detected spectra of LL-Chile (Fig. S6A) and LL-Pakis (Fig. S6B) acquired with B_1 optimized for $S=½$ also distinguish the signal for S_3^- from the underlying Mn^{2+} lines.

Similar to the behavior in UMB the CW spectrum of S_3^- in LL-Afghan (Fig. S7A) and LL-Chile (Fig. S7B) at 82 K also exhibit g anisotropy that was not observed at 295 K. A CW spectrum similar to that in Fig. S7A was previously attributed to Fe^{3+} [22], but analogy with spectra for S_3^- suggest this alternate assignment.

3.3 Distributions of Relaxation Times

A striking feature of the relaxation measurements for the S_3^- radical in the UMB, LL, and DMSO samples is the very wide distribution of relaxation times.

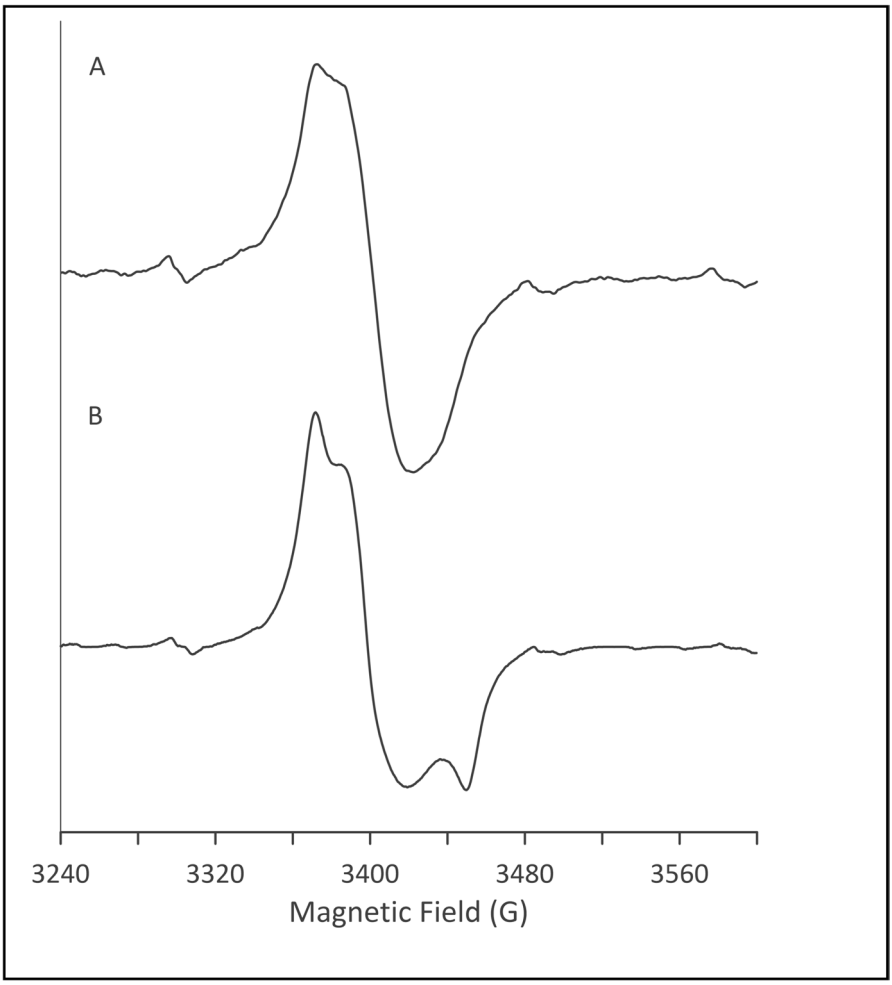

Fig. 3 The S_3^- radical signal was strong relative to the Mn^{2+} spectra in LL-Pakis at **A** 293 K and **B** 82 K. The decreased anisotropy at 293 K relative to 82 K is attributed to partial motional averaging

Exponential curves and in most cases biexponential curves did not fit the experimental data well. For the S_3^- signal in the solid samples the stretch exponent, β, for T_m (Eq. 1) varied from about 0.6 at 4 K to 1.0 at 75 K and for T_1 (Eq. 2) varied from about 0.3 at 4 K to 0.7 at 75 K. The values of β much less than 1.0 are indicative of a wide distribution of relaxation times. A similar trend was observed by Goslar et al. [6]. The distribution of spins in the lattice is unlikely to be uniform, and differences in inter-spin distances contribute to the range in relaxation times for both UMB and LL samples. For the solution in DMSO:dioxane β for fits to the inversion-recovery data varied from 0.64 at 4 K to 0.79 at 50 K. In the LL samples there are overlapping signals from S_3^- and Mn^{2+} (and possibly other species from the minerals) which contribute to the phase memory decay

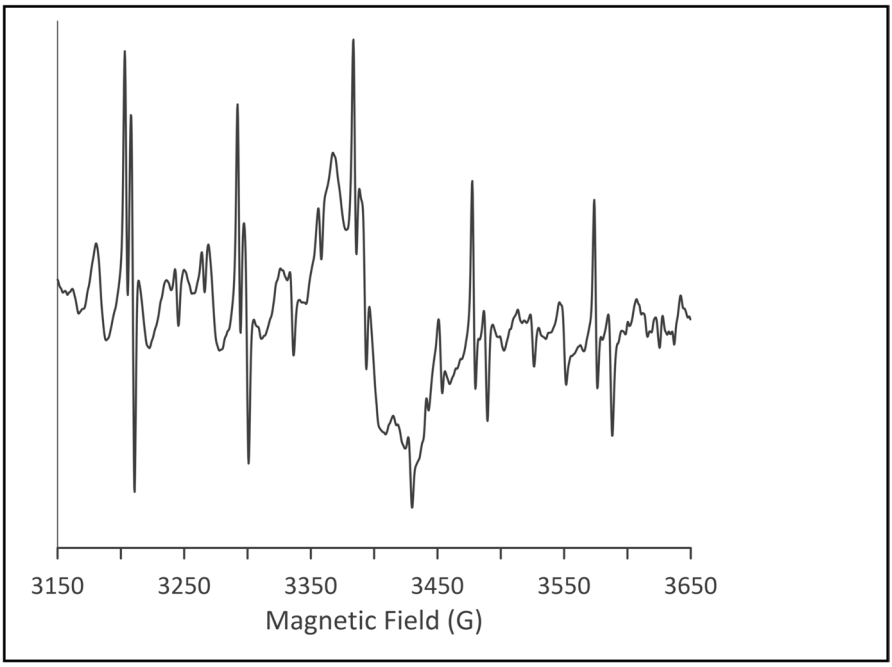

Fig. 4 Room temperature CW spectrum of LL-Chile illustrating the Mn^{2+} spectra overlapping the S_3^- spectrum

times and inversion-recovery times that are challenging to distinguish. Since the S_3^- spectrum is narrow relative to the width of the Mn^{2+} spectra we could measure the metal relaxation independent of the S_3^-, but not the S_3^- independent of the underlying Mn^{2+}. The width of the S_3^- radical spectrum made it feasible to measure relaxation times, and spin echo phases, at two well-separated field positions within the spectrum. By selection of temperatures, pulse-repetition rates, and pulse-turning angles the S_3^- or Mn^{2+} contributions could be emphasized. For Mn^{2+} the allowed or forbidden transitions could be selected. ESEEM was observed in 2-pulse echo decays of S_3^- but not of Mn^{2+}, which helped to identify contributions to overlapped spectra.

At 78 K T_1 increased and T_m decreased slightly when the $\pi/2$ pulse length was increased from 16 to 80 ns. This trend is not consistent with instantaneous diffusion or spectral diffusion, and may illustrate the changes in sampling of the range of relaxation times due to changes in the time window during which data can be acquired. Since the room temperature spectrum is approximately Lorentzian, it is assumed that spin exchange decreases T_m and that spectral diffusion is so fast within the line that the tests applied did not measure its rate. As motion slows at lower temperature, a wide range of relaxation times result from a range of motional effects on both dipole and exchange interactions. In addition, due to the superposition of Mn^{2+} and S_3^- spectra, changes in temperature and acquisition parameters can change the relative contributions to the relaxation measurements. This makes the usual plot of

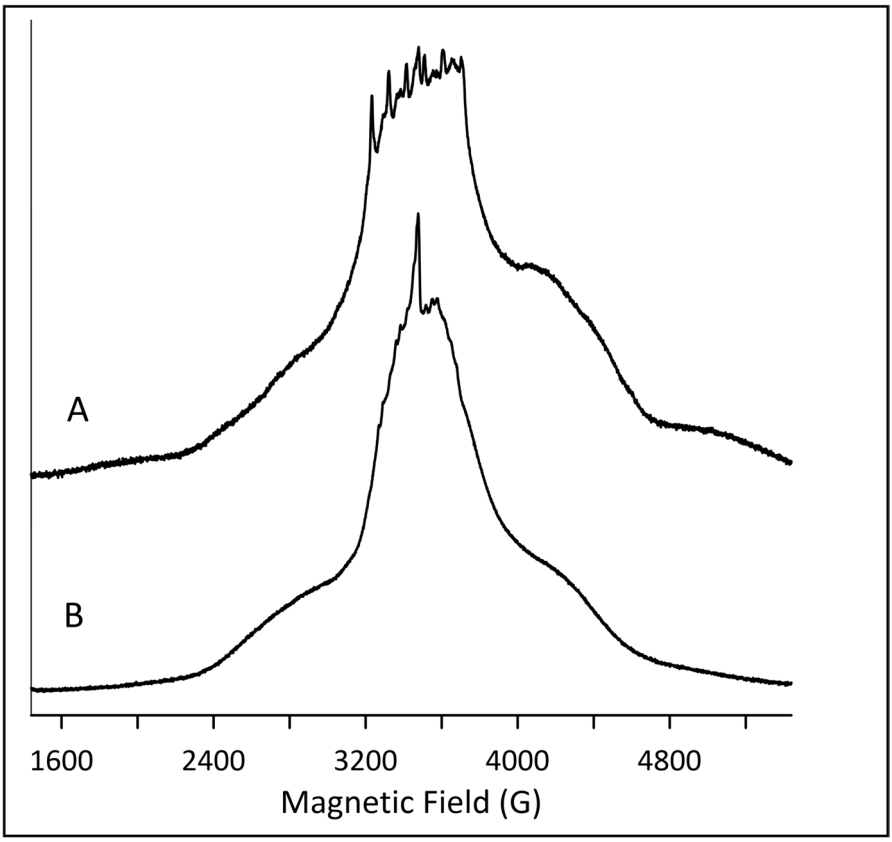

Fig. 5 Echo-detected spectrum of LL-Afghan at 41 K. The Mn^{2+} $\pm 1/2$ transitions can be seen near the maximum in this spectrum. **A** The pulse-turning angle was chosen to emphasize the $S = 5/2$ Mn^{2+} spin state. **B** The Mn^{2+} $\pm 1/2$ transitions are less visible in this spectrum. The pulse-turning angle was chosen to emphasize the $S = 1/2$ spin state. The "spike" near the maximum is not at the g value for S_3^- and might be an unknown defect or other radical in the mineral lattice. The S_3^- radical is not obvious in this spectrum

relaxation rate vs. temperature less meaningful for the mineral samples so only the data for LL-Chile are reported.

A UPEN [23, 24] analysis confirms that broad distributions in T_1 values occur at all temperatures measured. In some cases, there is more than one peak in the distributions, showing that double exponential fits at least roughly approximate the distributions. For example, at 5.2 K the double exponential fit yielded 3 and 22 μs at the center of the S_3^- spectrum. UPEN yielded 2 and 20 μs. The stretched exponential fit yielded 8.1 with a stretch factor of 0.59, and the geometric mean in UPEN was 5.2 μs. In almost all cases there was a very fast component of T_1 and T_m. The relaxation time values obtained depended very strongly on the starting time of the data. Excluding the first point or the first couple of points in the decay or recovery changed the weighting of the contribution of the shortest relaxation time. With

T_m values of the order of 200 ns, about half of the signal was missed within the dead-time of the instrument. Similarly, when T_1 is long, requiring several microsecond step sizes in the inversion-recovery data collection, fast recoveries are missed entirely. T_m measurements tended to become simple exponentials at high temperatures with values of about 160–220 ns. Shorter values would have been missed. At lower temperatures there was also a component slower by a factor of three or so. Another indication of incomplete sampling of the real full range of relaxation times is that in some cases the derived T_1 appeared to become longer when the sample temperature increased from 4.2 to 10 K. Physical models of the relaxation mechanisms are needed to account for this wide distribution of relaxation times.

3.4 Nuclear Modulation

The S_3^- signal in LL-Pakis exhibited long enough T_m to define nuclear modulation. Coupling to nuclei in the lattice was observed as modulation in 2-pulse echo decays when $\pi/2$ pulses were 80 ns or shorter. To record the modulation frequencies accurately, 3-pulse ESEEM was employed. The Fourier transform of our 3-pulse ESEEM data yielded a single frequency of 3.8 MHz at 3460 G, as expected for coupling to ^{23}Na and/or ^{27}Al. X-band HYSCORE showed coupling to ^{23}Na and/or ^{27}Al. Our results agree with those of Hoffmann et al. [6, 8–10] who measured modulation of the S_3^- echo decays at the ca. 3.8 MHz Larmor frequencies of ^{23}Na and ^{27}Al, which cannot be distinguished at X-band.

3.5 Temperature Dependence of Relaxation

The temperature dependence of T_m and T_1 for S_3^- in UMB-PB at high-field ($g = 2.007$) and low-field ($g = 2.046$) positions in the spectrum are presented in Fig. 6. Relaxation rates for the three UMB samples and for LL-Chile are compared in Fig. S8 and S9. The values plotted in the Figures are single exponential fits for T_m and stretched exponential fits for T_1. With the cautions about distributions of times in mind, we note that in general T_m values were similar, a few hundred ns, and nearly independent of temperature for the three UMB samples. T_m for the Mn^{2+} components in the mineral samples was short also, except that T_m at 4.2 K was 2.6 µs in LL-Colo, and 935 ns in LL-Chile. Goslar et al. [6] measured relaxation for S_3^- up to 50 K in UMB with spin concentrations of about 10^{17} spin/cm^3. Up to 12 K T_m was constant at 1.9 µs, which is longer than the ~ 400 ns in UMB-PB. When the concentration is about 10^{17} spins/cm^3 T_2 would be ~ 20 µs if the electron–electron dipole interaction dominated [25]. The ca. 2 µs T_m measured by Goslar et al. [6] show that another mechanism dominates, which could be reorientation of the anisotropic radical, taking excited spins off resonance [26]. Although the rigid-limit EPR spectra observed at low temperature was interpreted by Goslar et al. [6] as indicating that the S_3^- radical motion was largely stopped (other than the vibration) below ca. 77 K, low-amplitude librations can still impact T_m. Our T_m values in UMB were an order of magnitude shorter than observed by Goslar et al. [6]. If the 5×10^{20} spins per gram in our sample were uniformly distributed, the dipole–dipole contribution

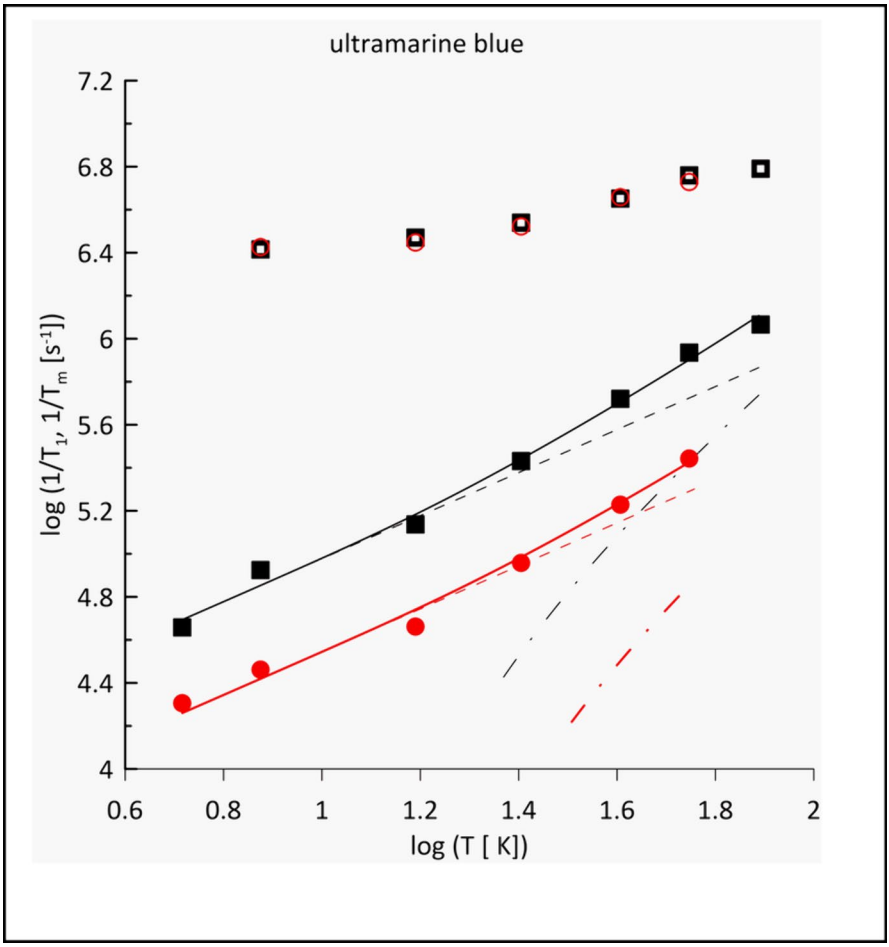

Fig. 6 Relaxation rates of the S_3^- radical in UMB-PB from 5.2 to 78 K at high-field ($g_x = 2.007$, red symbols and lines) and low-field ($g_y = 2.046$, black symbols and lines) positions in the spectrum (Fig. 1B). The values plotted for T_m (open symbols) are single exponential fits and for T_1 (closed symbols) are stretched exponential fits. The contributions from cross relaxation (dashed lines) and a Raman process (dash-dot lines) combine to give the fits (solid lines) to the experimental data as discussed in the text

would cause a T_2 of ca. 60 ns. We assume a non-uniform distribution. This is consistent with the very short T_m values in the distributions observed, and with the suggestion that some of the spins are not observed in the pulse experiments because T_m is so short. The non-observation of some spins due to short T_m also means that some T_1 values are not observed. For S_3^- in DMSO:dioxane T_m between 4 and 30 K was between 0.87 and 1 μs, which is longer than in the higher concentration UMB samples. At the low concentrations echo dephasing is attributed to low-amplitude librations.

Our T_m values are in reasonable agreement with prior reports on other types of ultramarines, given the wide distributions measured and their dependence on exactly

where in the spectrum they were measured. S_2^- and S_3^- radicals were measured in several green ultramarine pigments with various concentrations of radicals [18]. T_m for S_2^- in ultramarine green is less than about half a microsecond over the full temperature range studied. The short T_m limits the pulsed EPR measurements to temperatures below about 78 K [18]. At 4 K T_m was about 200 ns and T_1 ranged from 55 to 297 µs for S_3^-. T_1 of S_2^- ranged from 7 to 137 µs. Arieli et al. [27] reported three different environments for S_3^- radicals in UMB, with temperature dependent anisotropy, interpreted as indicating that motion of the radical occurs. Extensive pulsed EPR measurements were made in the liquid helium range, but relaxation times per se were not reported for direct comparison with our results. Spectral diffusion and very short T_m were observed in samples with higher spin concentrations.

As shown in Fig. 6 and also by Goslar et al. [6], T_1 for S_3^- in UMB is much shorter on the low-field side of the spectrum ($g = 2.0503$ which they label as g_y) than at the high-field side ($g = 2.0016$ which they label g_x). At 10 K Hoffmann et al. [8] found 0.33 ms along x and 0.13 ms along y and z. Using the labeling from Fig. 1 in Ref. [6], the z axis of the S_3^- radical is the principal axis of the C_{2v} symmetry point group. The y axis is in-plane and the x axis is perpendicular to the plane of the molecule. T_1 was longest for S_3^- in the UMB-Spec sample and shortest for the UMB-old sample, and only weakly temperature dependent (Figs. S8 and S9). The metals in the LL samples complicate the measurements because of the overlap of the spectra, but are not expected to have much effect on the actual relaxation times of the S_3^- radicals because the metals are in a different mineral component. Temperature dependence of T_1 for S_3^- in the mineral samples was small, as in the UMB samples. Using the fits to the stretched exponential, T_1 for two aliquots of the LL-Afghan mineral averaged 3.4 µs almost independent of temperature within scatter of data from 4.2 to 60 K. The extremes for the LL-Pakis were 9.6 µs at 10 K and 2.4 µs at 60 K. T_1 for the LL-Chile sample was 16 µs at 4.9 K and 4.1 µs at 60 K. The longest T_1 measured was for the LL-Colo sample at 4.9 K, 45 µs, which decreased to 9.8 µs at 20 K. The S_3^- signal was too weak relative to the Mn^{2+} background to measure the LL-Colo sample at higher temperatures. In 1:1 DMSO:dioxane the temperature dependence of T_1 for S_3^- (Fig. 7) is more strongly temperature dependent than in the highly concentrated UMB samples, which is expected for magnetically dilute samples.

3.6 Relaxation Mechanisms

The temperature dependence of $1/T_1$ for S_3^- in UMB-PB was modeled using Eqs. (3) and (4). The fits shown in Fig. 6 were obtained with a combination of cross relaxation and a Raman process with a Debye temperature of 55 to 60 K (~40 cm^{-1}). Equally good agreement with the data could be obtained by replacing the Raman process with a local mode with energy of 85 K (60 cm^{-1}). Because of the much higher spin concentrations our T_1 relaxation times in UMB (Fig. 6) are dominated by spectral diffusion via cross relaxation to a much greater extent than in the Goslar et al. study [6]. We digitized the Goslar et al. data from their Fig. 12 and fit the temperature dependence using Eqs. (3) and (4). We can fit their data with the same 40 cm^{-1} local mode energy as they reported. An equally

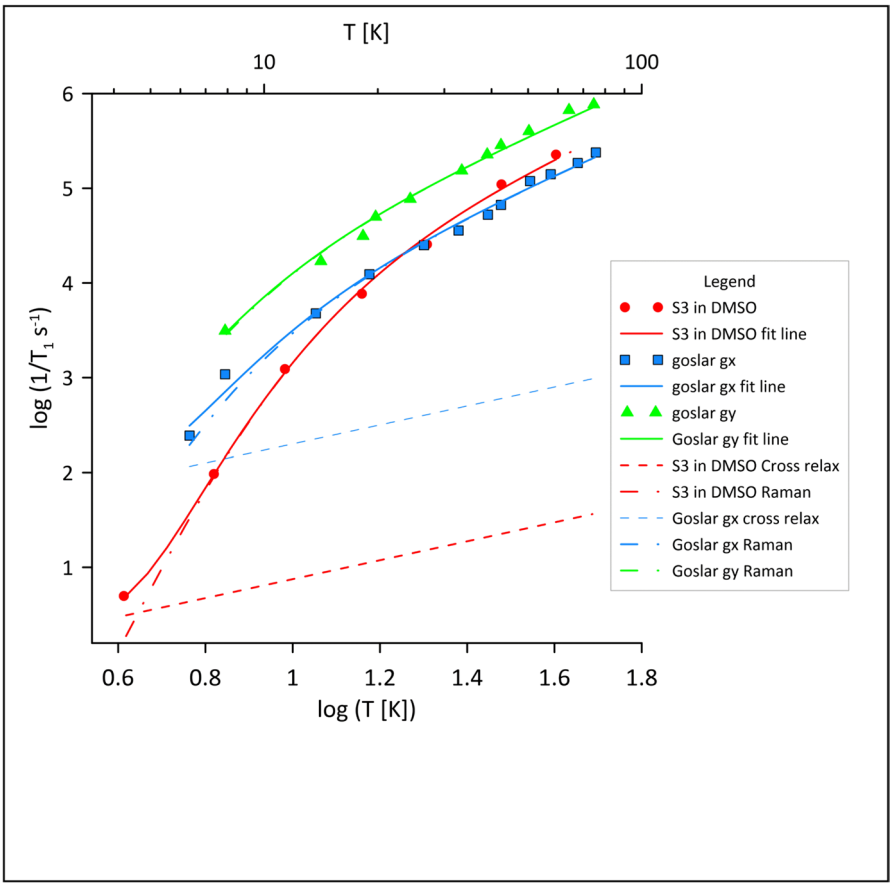

Fig. 7 Comparison of relaxation rates for 0.4 mM S_3^- in 1:1 DMSO:dioxane with literature values [6] in UMB sample with ~ 10^{17} spins/g; 1:1 DMSO:dioxane (red lines and symbols), along $g_x = 2.0016$ in UMB (blue lines and symbols), and along $g_y = 2.0503$ in UMB (green lines and symbols). The contributions from cross relaxation (dashed lines) and a Raman process (dash-dot lines) combine to give the fits (solid lines) to the experimental data

good fit was obtained with a Raman process and Debye temperature of 40–45 K (~ 30 cm^{-1}). The limited temperature range over which T_1 could be measured in prior studies and in the present study introduce substantial uncertainty to the mechanistic interpretation. The fitting with Eqs. (3) and (4) is based on matching the temperature dependence, which can be poorly defined over a small range. Cross relaxation makes much smaller contributions for the samples with lower spin concentration than in the synthetic UMB samples. In 1:1 DMSO:dioxane the temperature dependence of $1/T_1$ was well fit with a Raman process with Debye temperature of 70 K and a very small contribution from cross relaxation. Alternatively, the data in solution could be fit with a local mode with energy of 55 K.

The similarity in quality of fits to the data for a Raman process or local mode raises the possibility that multiple motional modes contribute to T_1. The wide distributions in relaxation rates also suggests that if a local mode dominates, there must be substantial uncertainty in the energy of that mode. In either case, the analyses indicate that relatively low-energy phonons dominate relaxation. One could speculate that these motions involve changes in the linear combinations of atomic orbitals on the central *S*, which would affect the in-plane *y* and *z* components more than the out-of-plane p_x orbitals. This is consistent with the faster T_1 in the *y* and *z* directions than in the *x* direction. Hoffmann et al. [8] summarized calculations that the orbital energies are sensitive to the bond angle, and stated that g_x is not sensitive to the angle, but g_z and g_y are sensitive to angle, thus explaining the anisotropy in T_1.

3.7 Comparison with Relaxation of SO_2^- and SO_3 Radicals

Relaxation times have recently been reported for SO_2^- and SO_3^- in $Na_2S_2O_4$, $Na_2S_2O_5$, and $K_2S_2O_5$ lattices [28]. The spin concentrations in those samples were between 4×10^{16} and 1.4×10^{17} spins/g, which is several orders of magnitude lower than for the commercial UMB samples. Even in these lower concentration samples wide distribution in relaxation times were observed which was attributed to non-uniform spin distributions [28]. The low spin concentrations contributed to much longer T_m at low temperatures than for S_3^- in UMB: 6 µs for SO_3^- and 14 µs for SO_2^-. Because of the lower spin concentrations cross relaxation had less impact on T_1 below about 25 K for SO_2^- or SO_3^- than was observed for S_3^- in UMB. T_1 for S_3^- in synthetic UMB is substantially shorter than for SO_2^- and SO_3^- [28]. Relaxation times are so long for SO_2^- and SO_3^- that spin echoes can be observed at 293 K, but for S_3^- echoes become difficult to detect above about 78 K. At 78 K T_1 for S_3^- was ~ 1 µs, whereas T_1 is ~ 125 µs for SO_2^- and ~ 900 µs for SO_3^-. Electron-spin relaxation has been observed to increase with increasing deviation of g from the free-electron value, which is attributed to increasing spin–orbit coupling [29, 30]. The spin lattice relaxation times at 78 K decrease in the order SO_3^- ($g_{avg}=2.0035$) < SO_2^- ($g_{avg}=2.006$) < S_3^- ($g_{avg}\sim2.028$). The faster relaxation for S_3^- is therefore attributed to increased spin–orbit coupling that also results in higher g value. The high mobility of S_3^- in the sodalite cages may also contribute to faster relaxation.

4 Conclusions

Commercial samples of UMB usually are not described by the vendor other than by color and a few other physical properties. The deep-blue pigments used in other studies are likely to be similar to the Pfaltz & Bauer pigment that we studied. As we demonstrated, the relaxation times for the S_3^- in the commercial samples can be very different from those of low-concentration samples because of cross relaxation. This is particularly evident at low temperatures where cross relaxation dominates relaxation at high spin concentrations. At ambient temperatures the rapid relaxation

of the EPR signal for S_3^- has the advantage that the signal is difficult to power saturate. This property is convenient for an EPR standard. The faster relaxation for S_3^- than for SO_2^- or SO_3^- is attributed to larger spin–orbit coupling.

Supplementary Information The online version contains supplementary material available at https://doi.org/10.1007/s00723-024-01716-1.

Acknowledgements This work was funded in part by the National Institutes of Health R01 CA262159 (GRE, PI), and in part by the University of Denver. Dr. Ralph T. Weber provided helpful information about his measurements of UMB-Spec and provided a sample. Dr. Brady Worrell called the lapis lazuli at the store in Crested Butte to our attention. Prof. Filipe Herrera and Mauricio Arias, Department of Physics, Universidad de Santiago de Chile provided the sample from the mine in Chile. Prof. Velavan Kathirvelu purchased the LL-Pakis at a shop in India. Samples of LL that were originally stated to be from a mine in India were eventually concluded to have originated in Pakistan.

Author Contributions SSE and GRE performed experiments, analyzed data, and wrote the manuscript. DGM prepared S_3^- in DMSO, recorded UV–VIS and EPR spectra, analyzed data, and assisted in editing the manuscript.

Funding National Institutes of Health, CA262159.

Data Availability Data are provided within the manuscript or supplementary information files.

Declarations

Conflict of interest The authors declare no competing interests.

References

1. F. Seel, Stud. Inorg. Chem. **5**, 67–89 (1984)
2. N.V. Chukanov, R.Y. Shendrik, M.F. Vigasina, I.V. Pekov, A.N. Sapozhnikov, V.D. Shcherbakov, D.A. Varlamov, Minerals **12**, 887 (2022)
3. D.M. Gardner, G.K. Fraenkel, J. Amer. Chem. Soc. **77**, 6399–6400 (1955)
4. V. Pinon, E. Levillain, J.P. Lelieur, J. Magn. Reson. **96**, 31–39 (1992)
5. G.R. Eaton, S.S. Eaton, J.W. Stoner, R.W. Quine, G.A. Rinard, A.I. Smirnov, R.T. Weber, J. Krzystek, A.K. Hassan, L.C. Brunel, A. Demortier, Appl. Magn. Reson. **21**, 563–570 (2001)
6. J. Goslar, S. Lijewski, S.K. Hoffmann, A. Jankowska, S. Kowalak, J. Chem. Phys. **130**, 204504 (2009)
7. G.E. Cutsall III., J. Telser, B.M. Hoffman, Biochim. Biophys. Acta **1853**, 1370–1394 (2015)
8. S.K. Hoffmann, J. Goslar, S. Lijewski, A. Jankowska, S. Kowalak, Microporous Mesoporous Mater. **127**, 205–212 (2010)
9. S.K. Hoffmann, J. Goslar, S. Lijewski, I. Olejniczak, A. Jankowska, A. Werbinska, S. Kowalak, Ind. Eng. Chem. Res. **49**, 8192–8199 (2010)
10. S.K. Hoffmann, J. Goslar, S. Lijewski, I. Olejniczak, A. Jankowska, S. Zeidler, S. Kowalak, Microporous Mesoporous Mater. **151**, 70–78 (2012)
11. H. Li, X. Tang, J.H. Pang, X. Wu, E.K.L. Yeow, J. Wu, S. Chiba, J. Amer. Chem. Soc. **143**, 481–487 (2021)
12. S.S. Eaton, G.R. Eaton, in *Relaxation Mechanisms*, eds. by D. Goldfarb and S. Stoll. EPR Spectroscopy: Fundamentals and Methods (Wiley, Chichester, UK, 2018), pp.175–192
13. J.W. Orton, *Electron Paramagnetic Resonance: An Introduction to Transition Group Ions in Crystals* (Gordon and Breach, NY, 1968)
14. A. Abragam, B. Bleaney, *Electron Paramagnetic Resonance of Transition Ions* (Oxford University Press, Oxford, 1970)
15. J. Murphy, Phys. Rev. **145**, 241–247 (1966)

16. A. Wieckowski, Phys. Stat. Solidi **42**, 125–130 (1970)
17. N. Gobeltz-Hautecoeur, A. Demortier, B. Lede, J.P. Lelieur, C. Duhayon, Inorg. Chem. **41**, 2848–2854 (2002)
18. K. Raulin, N. Gobeltz, H. Vezin, N. Touati, B. Lede, A. Moissette, Phys. Chem. Chem. Phys. **13**, 9253–9259 (2011)
19. M.C. Thurnauer, J.R. Norris, Chem. Phys. Lett. **76**, 557–561 (1980)
20. R. Carmieli, Q. Mi, A.B. Ricks, E.M. Giacobbe, S.M. Mickley, M.R. Wasielewski, J. Amer. Chem. Soc. **131**, 8872–8873 (2009)
21. M. Simenas, L. Macalik, K. Aidas, V. Kalendra, D. Klose, G. Jeschke, M. Maczka, G. Volkel, J. Banys, A. Poppl, J. Phys. Chem. **121**, 27225–27232 (2017)
22. N.B. Silva-Carrera, N.F. Cano, T.K. Gundu Rao, J.S. Ayala-Arenas, S. Watanabe, J. Lumin. **188**, 472–477 (2017)
23. G.C. Borgia, R.J.S. Brown, P. Fantazzini, J. Magn. Reson. **132**, 65–77 (1998)
24. G.C. Borgia, R.J.S. Brown, P. Fantazzini, J. Magn. Reson. **147**, 273–285 (2000)
25. B.T. Ghim, S.S. Eaton, G.R. Eaton, R.W. Quine, G.A. Rinard, S. Pfenninger, J. Magn. Reson. A **115**, 230–235 (1995)
26. J.L. Du, K.M. More, S.S. Eaton, G.R. Eaton, Israel J. Chem. **32**, 351–355 (1992)
27. D. Arieli, E.W. Vaughan, D. Goldfarb, J. Amer. Chem. Soc. **126**, 5776–5788 (2004)
28. G. Amassah, D.G. Mitchell, T.A. Hovey, S.S. Eaton, G.R. Eaton, Appl. Magn. Reson. **54**, 849–867 (2023)
29. H. Sato, S.E. Bottle, J.P. Blinco, A.S. Micallef, G.R. Eaton, S.S. Eaton, J. Magn. Reson. **191**, 66–77 (2008)
30. K. Chakarawet, M. Atanasov, J.D. Ellis, W.W. Lukens, V.G. Young, R. Chatterjee, F. Neese, J.R. Long, Inorg. Chem. **60**, 18553–18560 (2021)